


RESEARCH ARTICLE

Locally invasive, castrate-resistant prostate cancer in a *Pten*/*Trp53* double knockout mouse model of prostate cancer monitored with non-invasive bioluminescent imaging

Courtney Yong¹ , Devon L. Moose² , Nadine Bannick², Wade R. Gutierrez^{3,4} , Marion Vanneste², Robert Svensson^{2a}, Patrick Breheny⁵, James A. Brown¹, Rebecca D. Dodd^{3,6}, Michael B. Cohen⁷, Michael D. Henry^{1,2,6,8,9*}

1 Department of Urology, Carver College of Medicine, University of Iowa, Iowa City, IA, United States of America, **2** Department of Molecular Physiology and Biophysics, Carver College of Medicine, University of Iowa, Iowa City, IA, United States of America, **3** Department of Internal Medicine, Carver College of Medicine, University of Iowa, Iowa City, IA, United States of America, **4** Medical Scientist Training Program, Carver College of Medicine, University of Iowa, Iowa City, IA, United States of America, **5** Department of Biostatistics, College of Public Health, University of Iowa, Iowa City, IA, United States of America, **6** Holden Comprehensive Cancer Center, University of Iowa, Iowa City, IA, United States of America, **7** Department of Pathology, Wake Forest School of Medicine, Winston-Salem, NC, United States of America, **8** Department of Pathology, Carver College of Medicine, University of Iowa, Iowa City, IA, United States of America, **9** Department of Radiation Oncology, Carver College of Medicine, University of Iowa, Iowa City, IA, United States of America

 These authors contributed equally to this work.

 Current address: Nimbus Therapeutics, Cambridge, MA, United States of America

* michael-henry@uiowa.edu

Abstract

Here we have improved an existing mouse model of prostate cancer based on prostate-specific deletion of *Pten* and *Trp53* by incorporating a Cre-activatable luciferase reporter. By coupling the deletion of those genes to the activation of a luciferase reporter, we were able to monitor tumor burden non-invasively over time. We show that, consistent with previous reports, deletion of both *Pten* and *Trp53* on a C57BL/6 background accelerates tumor growth and results in both the loss of androgen receptor expression and castrate resistant tumors as compared with loss of *Pten* alone. Loss of *Trp53* results in the development of sarcomatoid histology and the expression of markers of epithelial-to-mesenchymal transition Zeb1 and vimentin, with kinetics and penetrance dependent on whether one or both alleles of *Trp53* were deleted. Homozygous deletion of *Trp53* and *Pten* resulted in uniformly lethal disease by 25 weeks. While we were able to detect locally invasive disease in the peritoneal cavity in aggressive tumors from the double knockout mice, we were unable to detect lymphatic or hematogenous metastatic disease in lymph nodes or at distant sites.



OPEN ACCESS

Citation: Yong C, Moose DL, Bannick N, Gutierrez WR, Vanneste M, Svensson R, et al. (2020) Locally invasive, castrate-resistant prostate cancer in a *Pten*/*Trp53* double knockout mouse model of prostate cancer monitored with non-invasive bioluminescent imaging. *PLoS ONE* 15(9): e0232807. <https://doi.org/10.1371/journal.pone.0232807>

Editor: Irina U. Agoulnik, Florida International University, UNITED STATES

Received: April 21, 2020

Accepted: September 10, 2020

Published: September 28, 2020

Copyright: © 2020 Yong et al. This is an open access article distributed under the terms of the [Creative Commons Attribution License](https://creativecommons.org/licenses/by/4.0/), which permits unrestricted use, distribution, and reproduction in any medium, provided the original author and source are credited.

Data Availability Statement: All relevant data are within the paper and its Supporting Information files.

Funding: This work was supported in part by R21 CA137490 (to MDH) and the Andersen-Hebbeln Chair funds (to JAB). Core facilities used in these studies were supported by the Holden Comprehensive Cancer Center support grant P30 CA086862. The funders had no role in study

design, data collection and analysis, decision to publish, or preparation of the manuscript.

Competing interests: The authors have declared that no competing interests exist.

Introduction

Prostate cancer is the most commonly diagnosed malignancy in men worldwide [1]. While the 5-year survival rate is high overall and has improved with prostate specific antigen (PSA) screening guidelines and new treatment modalities, it is still the second leading cause of cancer deaths for men in the United States [2]. Although most prostate cancers are found while the disease is still localized, for those with metastatic dissemination the 5-year survival drops to approximately 30% [2]. Two of the most commonly altered pathways in metastatic prostate cancer are PI3K-AKT and p53. The PI3K-AKT axis is hyperactive in prostate cancer through the deletion of its negative regulator and tumor suppressor gene, phosphatase and tensin homolog on chromosome 10 (*PTEN*). *PTEN* mutations occur at a frequency of approximately 17% in primary tumors and is increased to near 40% in metastatic tumors [3, 4]. Mutations in and amplification of the PI3K catalytic subunits are also observed. *TP53* mutations occur in approximately 7% of primary tumors and 50% of metastases [3, 4]. Other mutations that occur at an elevated frequency in metastatic disease are in the retinoblastoma, *MYC*, and androgen receptor pathways [3, 4].

The first genetically engineered mouse model for prostate cancer was the TRAMP model [5]. TRAMP mice are engineered for prostate-specific expression of both the large and small T-antigen, which results in the inhibition of *Trp53* and *Rb1* as well as the activation of AKT. While this model exhibits metastasis, its pathology more closely reflects rare high-grade, neuroendocrine-like disease [6, 7]. In an attempt to build better models of prostate cancer, investigators have utilized prostate-specific, conditional gene knockout strategies [8].

Homozygous deletion of *Pten* using Cre recombinase controlled by a prostate-specific probasin promoter initially demonstrated lethal metastatic prostate cancer in mice [9]. However, subsequent efforts found indolent disease in prostate-specific *Pten* knockout mice extensively backcrossed onto the C57BL/6 background [10, 11]. Chen, *et al.* showed that combining deletion of *Trp53* with *Pten* on a C57BL/6 background unleashed a more aggressive, lethal phenotype with mice succumbing to bulky, locally invasive tumors [11]. Martin, *et al.* expanded on those findings and demonstrated that the prostate specific dual deletion of *Trp53* and *Pten* resulted in rapid progression from prostate intraepithelial neoplasia to adenocarcinoma and ultimately sarcomatoid pathology, coupled with a progressive decrease in androgen receptor staining [12]. More recently, the Goodrich group has combined deletion of *Rb1* with *Pten* and/or *p53* resulting in aggressive, metastatic disease including bone metastasis [13]. The addition of a *Trp53* deletion conferred castrate-resistance to the *Rb1*; *Pten* knockout tumors [13]. However, with the deletion of *Rb1* in this model, the resulting disease more closely resembled high-grade neuroendocrine prostate cancer.

We have previously described a prostate-specific *Pten* knockout mouse with a genetically engineered luciferase reporter that allowed quantitative, noninvasive monitoring of disease progression [10]. However, as mentioned above, this model did not develop metastatic disease, and castration resulted tumor regression with no relapse. Here we have combined loss of *Trp53* with *Pten* with a luciferase reporter on an extensively backcrossed albino C57BL/6 background to facilitate bioluminescence imaging (BLI). We show that these mice rapidly develop fatal, bulky, locally invasive tumors. We also note the consistent development of sarcomatoid pathology and epithelial-to-mesenchymal transition (EMT)-like features in these tumors. Despite the presence of these features, we did not detect disseminated metastatic disease via BLI or histologic analysis, supporting previous findings with this model.

Materials and methods

Mouse strains and genotyping

All animal procedures were performed under approval from the Institutional Animal Care and Use Committee at the University of Iowa, AP #1302028. Animals were housed in standard conditions following guidelines outlined in PHS Animal Welfare Assurance (D16-00009, A3021-01) and United States Department of Agriculture (USDA No. 42-R-0004). Mice were housed in Thoren individually ventilated cages that contained SoftZorb Enrichment Blend bedding (Northeastern Products Crop, Warrensburg, NY), had 24 hr access to 0.2 μ m filtered water via Edstrom automatic watering system, and fed Teklad 7913 irradiated diet (Harlan). We crossed homozygous albino C57BL/6J-Tyr^{c-2J}/J ROSA26 LSL-Luc Pten^{fl/fl} generated from our previous studies [10] mice with heterozygous B6.129P2-Trp53^{tm1Brn}/J (Jackson Laboratory), as well as with B6.Cg-Tg(Pbsn-cre)4Prb (Pb-Cre4⁺) mice obtained from the NIH Mouse Models of Human Cancer Consortium. The mice were selected for Pten^{fl/fl} and either Trp53^{fl/+} or Trp53^{fl/fl}. Once the desired alleles were obtained, mice were backcrossed to C57BL/6J-Tyr^{c-2J} (Jackson Laboratory) mice for six generations, selecting for albino-coat color offspring. Mice were genotyped for Cre, floxed alleles of Pten, Trp53, and luciferase as described previously [14–17]. Three groups of males were generated yielding 15 wild type Trp53 mice with homozygous Pten deletion (WT), 17 mice heterozygous for Trp53 with homozygous Pten deletion (HET), and 16 double knockout mice (DKO) for a total of 48 mice. Additionally, 5 more DKO mice had undergone surgical castration to study the response to androgen deprivation. Mice were examined and imaged starting at five weeks of age. Mouse health was monitored 3 times weekly and mice were euthanized by gas CO₂ followed by cervical dislocation if body scores were 2 or less [18], or if they displayed signs of declining health such as decreased mobility. Three mice died before meeting experimental endpoints.

Bioluminescence imaging

All bioluminescence imaging (BLI) was performed using an Ami HTX imager from Spectral Instruments Imaging (Tucson, AZ). Animals were anesthetized in a chamber with 3.5% isoflurane, and then 150 mg/kg D-luciferin (VivoGlo, Promega, Madison, WI) was injected intraperitoneally. Mice were then placed into the imager while maintaining anesthesia and an image was obtained five minutes after D-luciferin injection. Exposure time was five minutes per image. AMIView Imaging Software, version 1.5.0 was used to analyze the region of interest and measure photon flux (photons/sec/cm²/sr). Images were obtained on *ex vivo* necropsy tissues shortly after necropsy with an additional five-minute exposure time.

Mouse examinations

All mice were examined and weighed bi-weekly. Examination included palpation of the abdomen and pelvis and evaluation of overall health and hygiene. Mice were imaged bi-weekly. Mice were euthanized according to pre-determined endpoints, including 20% loss of starting body weight, decreased mobility, lack of grooming, or other morbidity. Homozygous *Pten* deleted, wild type *Trp53* mice were euthanized alongside double knockout mice regardless of health status as an age-matched control. Additional cohort of *Pten* knockout mice were aged and euthanized alongside *Trp53* heterozygous mice as age matched controls for those mice. Necropsy included removal of the primary prostate tumors, imaging of the remainder of the animal, and subsequent removal of any bioluminescent tissues. Tissues were fixed in 10% neutral buffered formalin at 4°C for 24–48 hours and then dehydrated and embedded in paraffin.

Histopathology

Formalin-fixed, paraffin-embedded tissues were sectioned and stained using standard hematoxylin and eosin stains. Immunohistochemistry was performed on serial sections with the following antibodies: cytokeratin pan antibody cocktail (ThermoFisher, Waltham, MA; catalog #MA5-13203), androgen receptor (AR) (AbCam, Cambridge, UK; catalog #ab133273), vimentin (Cell Signaling Technology, Danver, MA; catalog #5741S), Zeb1 (obtained as a generous gift from the Richer lab at the University of Colorado) [19], and smooth muscle actin (SMA) (Bio-Rad, Hercules; CA catalog #MCA5781GA). Immunohistochemistry protocol included a heat-based antigen retrieval in 0.1 mM citrate buffer (pH 6.0), quench with 10% hydrogen peroxide, and blocking with 5% goat serum for all antibodies except for AR, which was blocked with 1.5% horse serum. The primary antibodies were then introduced at dilutions of 1:100 for cytokeratin, 1:250 for AR, 1:100 for vimentin, 1.5:1000 for Zeb1, and 1:500 for SMA. Slides were finally incubated in either horseradish peroxidase-conjugated (HRP) goat anti-rabbit (Jackson ImmunoResearch Laboratories, West Grove, PA; catalog #AB_2307391) or EnVision + HRP anti-mouse (Dako, Carpinteria, CA; catalog #K400111-2) secondary antibodies and developed using DAKO DAB. The slides were interpreted by a single pathologist with expertise in rodent models of prostate cancer who was blinded to genotype. Analysis for EMT status was determined by overlapping regions of Zeb1 and Vimentin positivity.

RNA extraction and RT-qPCR

RNA was isolated from 5 μ m thick whole-tissue FFPE sections as previously described [20]. Tissue sections were deparaffinized by washing twice with 1 mL of xylene, vortexed, and centrifuged (16,000 g x 5 min). Pellets were washed twice with 1 mL of 95% ethanol prior to RNA extraction. RNA extraction was performed using the RNeasy FFPE Kit (Qiagen, Valencia, CA; catalog #73504) according to the manufacturer's instructions. RNA integrity was determined using the 2100 Bioanalyzer (Agilent, Santa Clara, CA) and for RNA used in downstream applications the RIN was assessed to be ≥ 1.8 . Reverse transcription was performed on 750 ng of RNA with iScript cDNA Synthesis Kit (BioRad, Hercules, CA; catalog #). Quantitative PCR was performed using the PowerUp SYBR Green Master Mix (Applied Biosystems, Waltham, MA; catalog #A25780), according to manufacturer's guidance. Primers were designed using NCBI following the guidance on downstream applications from Qiagen. Expression of *Foxa2* (GGAAATGAGAGGCTGAGTGG; AAGTGTGGTGGCTACTTTTCCT), *Syp* (CGTTAAAGGGGGCACTACCA; TTCAGCCGAGGAGGAGTAGT), *Msmb* (CAATTCACCCAGAGAAGTGC; CCTGGGTCTTCCGATCCAC), and *Apof* (CTCTCTGGCTGAAGTCGAACA; GGGTTGAGAA GTAGAACTGTGC) were compared to the rRNA control 18S (GAGGCCCTGTAATTGGAATGAG; GCAGCAACTTTAATATACGCTATTGG).

Statistical analysis

Statistical analyses were performed with GraphPad Prism software 8.0. and R 3.6.3. Growth rates were analyzed by response feature analysis through fitting the growth data for each mouse individually to an exponential growth model, obtaining estimates of the rate parameters via nonlinear least squares. The growth rates were then compared using a one-way ANOVA with Tukey's honest significant differences used to correct for multiple comparisons. Survival data was analyzed using the Kaplan-Meier method. Pathologic data was qualitatively characterized and analyzed using Chi-squared tests with a Bonferroni correction for multiple hypothesis testing. RNA expression data was compared using a T-test to compare the delta Ct values. Data for gene expression is presented as a fold-change (2 exponent of the delta delta Ct) with SEM error bars.

Results

Prostate specific deletion of Trp53 and Pten leads to fast-growing, lethal, sarcomatoid tumors

To non-invasively monitor tumor burden, bioluminescence imaging (BLI) was performed on mice with Probasin-Cre mediated deletion of *Pten* and *Trp53*, coupled with the activation of a ROSA-LSL luciferase reporter. In this study, all mice had homozygous floxed *Pten* alleles, with cohorts having wildtype *Trp53* (WT), heterozygous floxed/wildtype *Trp53* (HET), or homozygous floxed *Trp53* alleles (DKO). The longitudinal BLI imaging (**Fig 1A and 1B**) demonstrated that tumors grew faster in the DKO mice than those in the HET and WT group (**S1A Fig**). After an initial rapid growth phase in all groups from 5–10 weeks, which reflects pubertal activation of Cre and growth of the prostate, WT mice showed little growth out to 50 weeks consistent with our previous studies [10]. For reference, mice in this strain lacking Cre expression do not show any BLI signal above background [17]. Notably, the BLI growth curves of the *Pten*-only deleted animals are remarkably similar as reported here and in our previous study despite the fact that they were measured in separate experiments conducted many years apart and on different imaging systems, here on an AMI HTX and previously on an IVIS 100 [10]. The DKO mice showed rapid tumor growth around 19 weeks of age that resulted in formation of readily palpable primary tumors and a median survival of 26.5 weeks (**Fig 1B and 1C**). These tumors were larger in comparison to the prostates of WT mice taken down at the same time-point (**S1B and S1C Fig**). In comparison to the DKO group, the HET group demonstrated slower disease progression with tumor growth not increasing until mice were around 29 weeks of age (**Fig 1B**). Moreover, the median survival for heterozygous *Trp53* null mice was closer to that of WT (41 and 50 weeks, respectively) (**Fig 1C**).

We performed histopathological analysis of prostates collected from DKO, HET, and WT mice euthanized at 25 weeks of age, as well as HET and WT mice at ~40 weeks (**Fig 2A**). At 25 weeks, 13/13 mice from the DKO group demonstrated sarcomatoid tumors as confirmed by negative staining with a pan-cytokeratin antibody, with most of the HET and WT showing high-grade mouse prostate intraepithelial neoplasia (HG mPIN) features. For the WT group, there was no difference in this distribution at 40 weeks; however, for the HET group, 6/6 tumors evaluated were sarcomatoid (**Fig 2B**). To rule out potential stromal expansion as the cause for the lack of cytokeratin staining in the mice presenting with sarcomatoid pathology, we stained for smooth muscle actin (SMA). In WT mice at 40 weeks of age, anti-SMA antibody stains the fibromuscular stroma surrounding glands with mPIN lesions. In contrast, in KO mice at 25 weeks of age or HET mice at 40 weeks of age, although there are some small, isolated patches of SMA staining, the bulk of these large tumors are SMA negative (**Fig 2A**).

Based on the histological characterization, we wished to determine if loss of *Trp53* lead to elevated EMT-like features in the tumors. For this we stained tissue for the EMT markers Zeb1 and vimentin (**Fig 3A**). For tumors to be scored positive for EMT, we applied the strict criteria that regions of overlapping positivity on serial sections for both markers are present. From this analysis, we observed an increase in EMT-positive tumors in the DKO group at 25 weeks of age as compared to the WT group (**Fig 3B**). As evident in **Fig 3A**, there were examples of some tumors in both WT and HET mice that showed some positive Zeb1 staining, but not vimentin staining which we scored negative for EMT. We analyzed a smaller group of HET and WT tumors at 40 weeks of age and although not statistically significant, we observed EMT-positive tumors in HET mice, but not WT mice (**S2 Fig**). We also asked if the loss of *Trp53* with *Pten* lead to an increase in neuroendocrine-like (NE) features. To achieve this we compared the expression of the prostate NE genes *Foxa2* and *Syp* mRNA by RT-qPCR between 5 DKO mice and 5 WT mice that were euthanized at 25 weeks of age (**Fig 3C**) [21, 22]. From this analysis

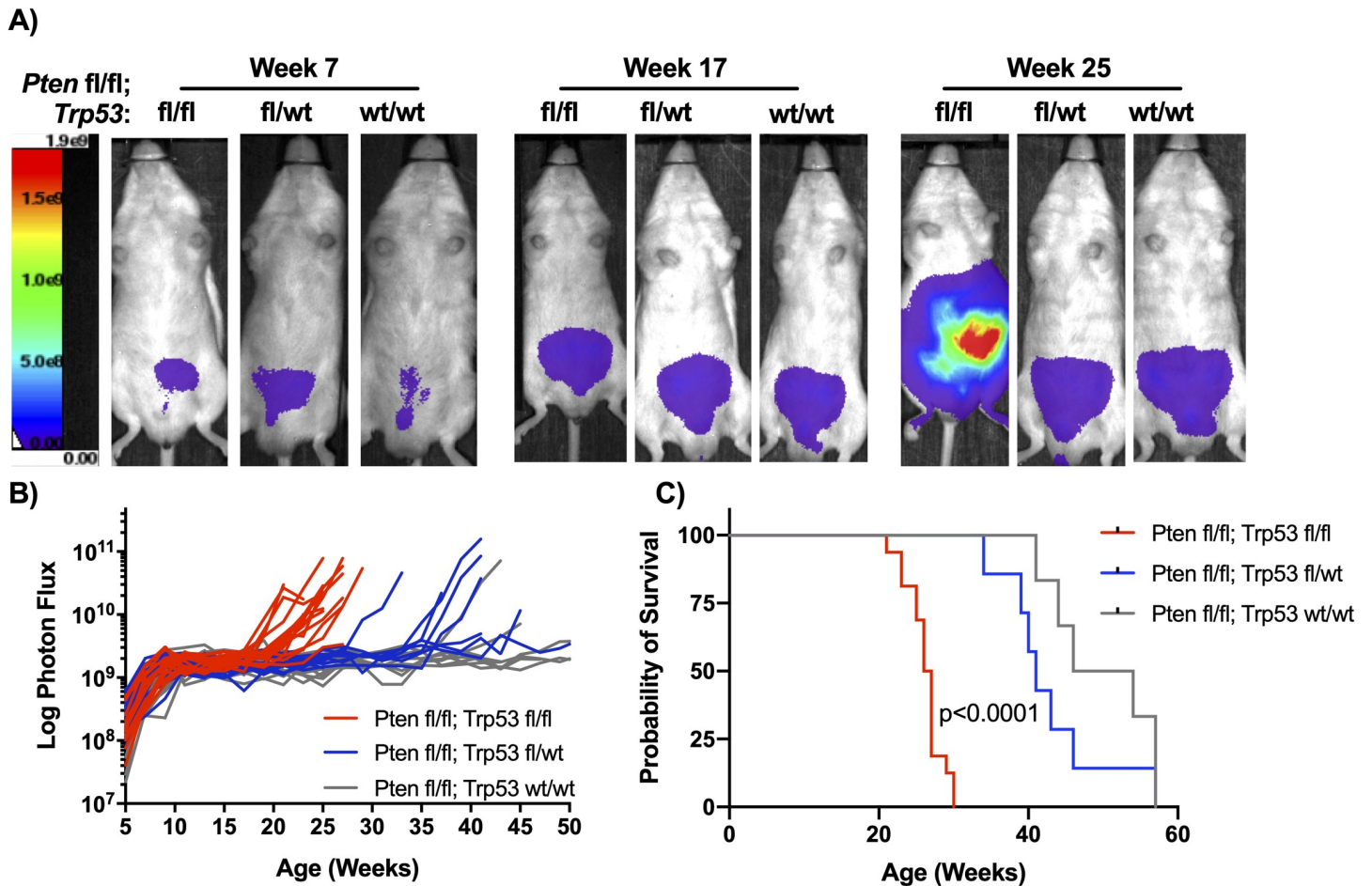


Fig 1. Combined loss of Trp53 and Pten accelerates prostate tumor growth. (A) Serial bioluminescence imaging (BLI) of mice with loss of *Pten* and wildtype *Trp53* (WT; wt/wt), heterozygous (HET; wt/fl), or homozygous (DKO; fl/fl) deletion of *Trp53*. (B) BLI signal development over time of each of the groups. BLI signal grew faster in the DKO than WT or HET mice ($p < 0.01$). (C) Kaplan-Meier curves showing DKO mice have decreased survival compared to WT and HET mice ($p < 0.0001$) ($n = 16$ for DKO; $n = 7$ for HET; $n = 6$ for WT).

<https://doi.org/10.1371/journal.pone.0232807.g001>

we observed a non-statistically significant trend towards a moderate increase in *Foxa2* and *Syp* expression, suggesting that there may be isolated regions of NE-like differentiation present in the DKO tumors, consistent with the heterogeneous expression of *Syp* observed previously in *Pten*; *Trp53* knockout mice [12].

Pten/Trp53 double knockout mice develop locally invasive disease but not lymphatic or distant metastasis

Due to the aggressive nature of the tumors from the DKO group and the prevalence of *PTEN* and *TP53* mutations in metastatic disease, we determined if there was metastatic disease in these mice. We evaluated residual tumor burden by BLI post-necropsy, after removal of the primary prostate tumor for 10 out of 16 mice (Fig 4A, 4D and 4F). This was necessary because the intense signal from the primary tumor could obscure weaker signals emanating from metastatic sites. We observed intraperitoneal spread in 8 out of 10 mice. We then histologically evaluated BLI signal-positive tissue to determine if there was metastatic disease (Fig 4B, 4C,

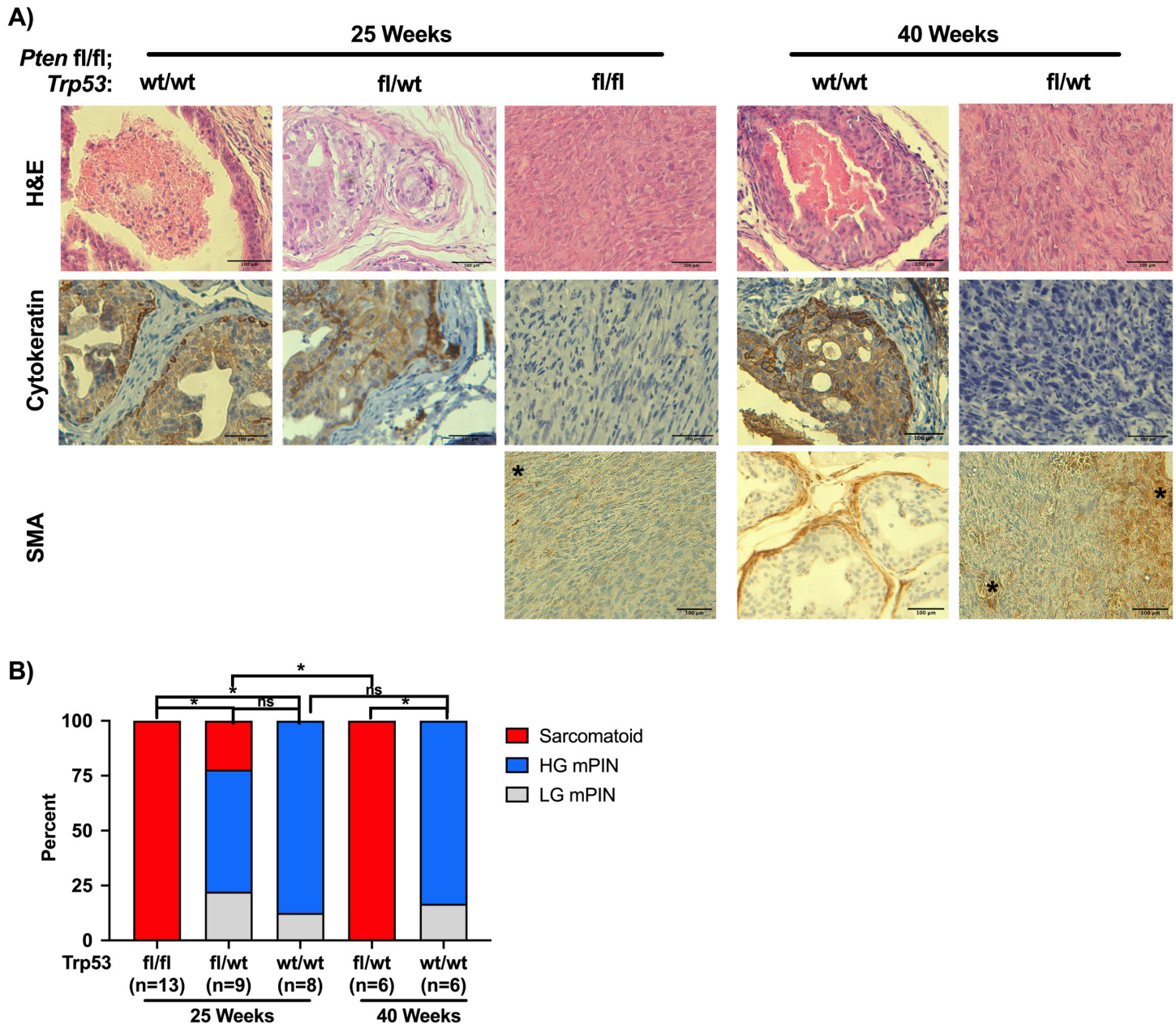


Fig 2. Histopathology analysis of WT, HET, and DKO tumors. (A) Representative sections of tissue from DKO mice, as well as both HET and WT at 25 and ~40 weeks. Disease stage was determined by pathologist review of H&E sections, with sarcomatoid being confirmed with a negative pan-cytokeratin stain. Bar = 100µm. Asterisks denote small patches of SMA-positivity. (B) Histopathology analysis from H&E and cyokeratin staining in (A), (* $p > 0.05$; Chi-Square with Bonferroni correction).

<https://doi.org/10.1371/journal.pone.0232807.g002>

4E and 4G). Upon histological evaluation of a mouse that appeared to have lumbar lymph node involvement (**Fig 4A**), we found that instead of intralymphatic growth, the tumor invaded into the local perilymphatic fat (**Fig 4B and 4C**). DKO mice (8/10) were found to have visceral BLI signal upon post-necropsy imaging (**Fig 4D**), but this seems more likely to be peritoneal seeding and local invasion than hematogenously-disseminated disease (**Fig 4E**). There was also evidence of aggressive, invasive disease with BLI-positive tumor invading into pelvic sidewall musculature (**Fig 4F and 4G**).

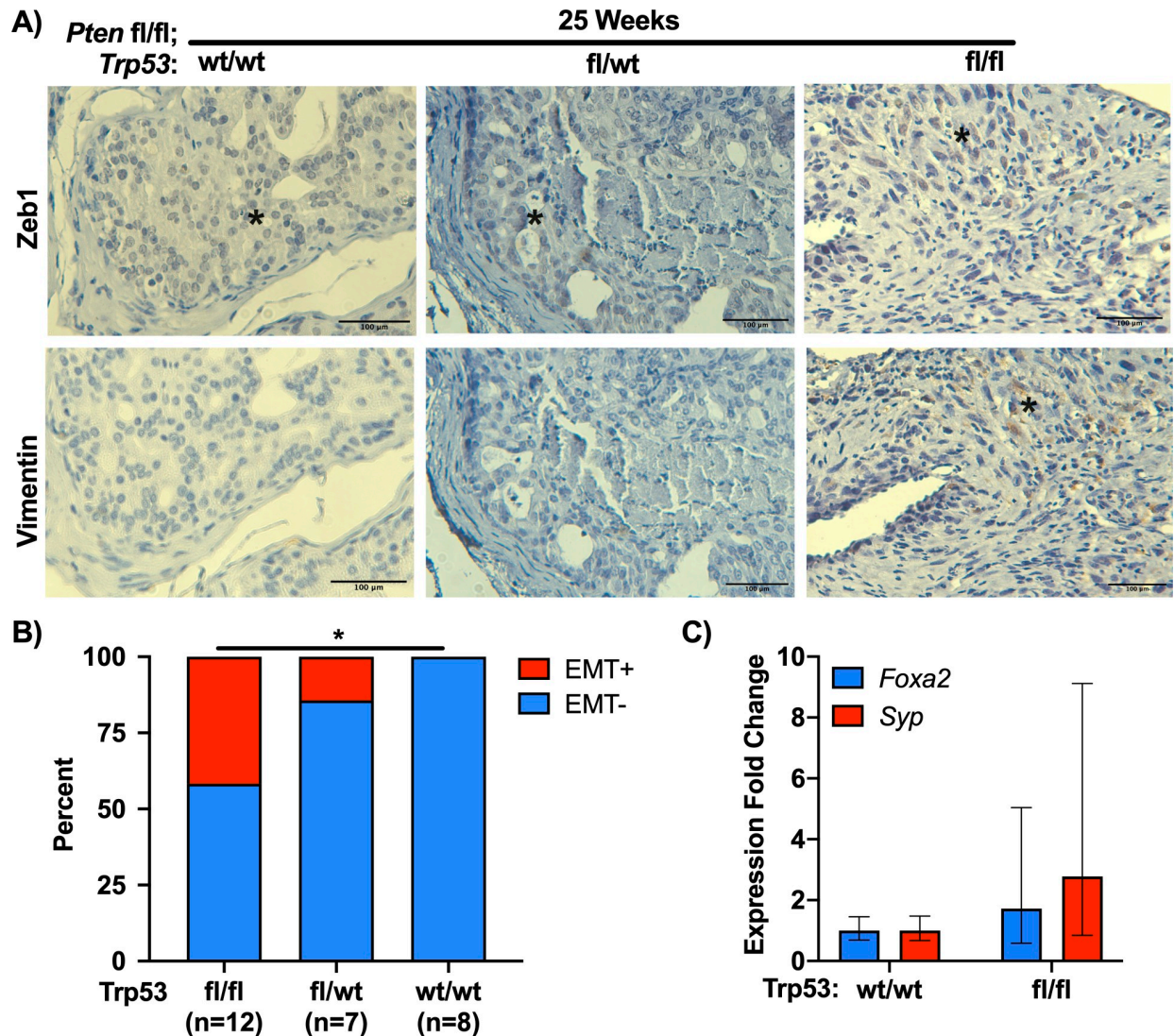


Fig 3. Pten;Trp53 double knockout tumors have EMT-like characteristics. (A) Immunohistochemistry for Zeb1 and Vimentin expression at 25 weeks of age. Asterisks indicate positive staining. Bar = 100 μ m. (B) Analysis of Zeb1 and Vimentin staining from (A), with EMT positive (EMT+) tissue having areas of overlapping Zeb1 and Vimentin staining in serial sections (* $p > 0.05$; Chi-Square). (C) Analysis of the neuroendocrine prostate markers Foxa2 and Synaptophysin (*Syp*) between 5 mice from WT (*Pten*^{fl/fl}; *Trp53*^{wt/wt}) and DKO (*Pten*^{fl/fl}; *Trp53*^{fl/fl}) at approximately 25 weeks of age ($p > 0.05$, t-test).

<https://doi.org/10.1371/journal.pone.0232807.g003>

Pten/Trp53 double knockout results in loss of androgen receptor expression and castrate resistant tumors

While the DKO tumors were not metastatic, we wished to investigate the androgen sensitivity of this model. To assess this, we generated a cohort of five DKO mice which were surgically castrated at 10 weeks of age. After castration, the BLI signal noticeably decreased between 10 and 15 weeks of age (Fig 5A). Eight weeks after castration, the tumor burden started to increase in all mice, demonstrating castrate-resistant prostate cancer. Histological analysis from these tumors revealed that, like the intact DKO mice, they were all sarcomatoid (S3A and S3B Fig). Due to the rapid and uniform onset of castrate-resistant growth, we determined if the tumors from intact mice demonstrated alterations in AR expression (Fig 5B and 5C).

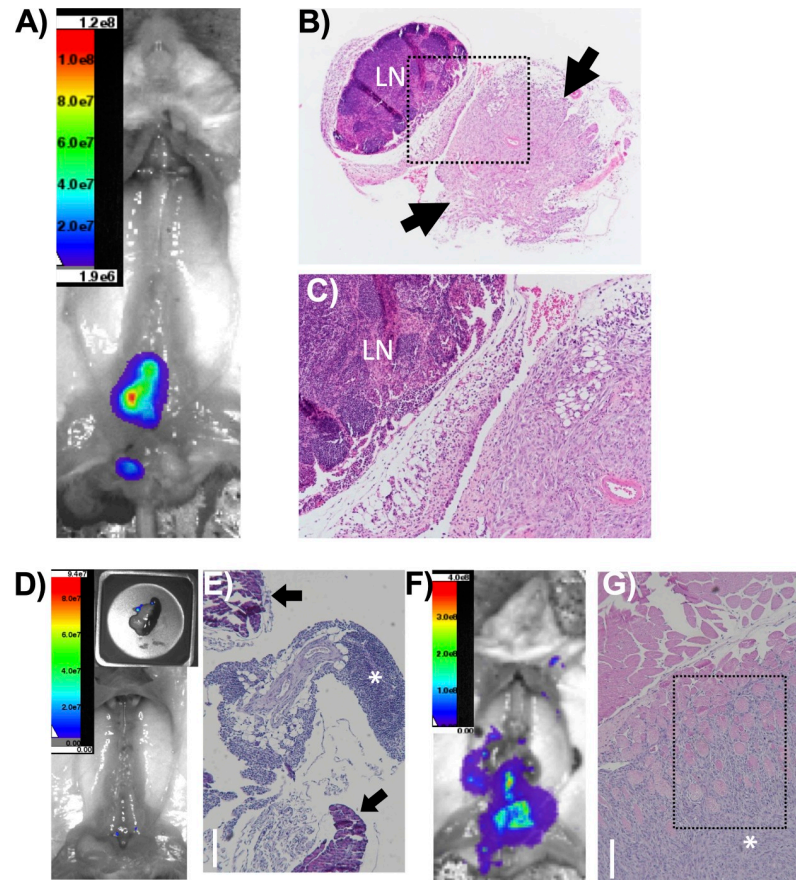


Fig 4. Loss of Pten and Trp53 results in locally invasive, but not metastatic disease. (A) Post-necropsy imaging in a DKO mouse. In situ, lymph nodes are BLI positive. (B-C) H&E stain showing a pelvic lymph node (LN) dissected at necropsy from the mouse in (A). The arrows represent areas of adjacent, locally invasive tumor. The area outlined by the black box in (B) is magnified in (C). (D) Post-necropsy imaging in a DKO mouse, with pancreas imaged separately (inset), with a nodule of tumor cells on the pancreas. (E) H&E stain showing the nodule dissected from the BLI-positive pancreatic lesion in (D). The tumor is indicated by the asterisk, and normal pancreatic tissue is marked with black arrows. The tumor is locally invasive into the tissue around the pancreas but not into the pancreatic tissue. (F) Post-necropsy imaging in a DKO mouse. The area near pelvic lymph nodes is BLI positive. (G) H&E stain of an area of BLI positivity in the mouse in (F). There is no lymphoid tissue, and the tumor (asterisk) is locally invasive into the adjacent muscle (black box). Bars in E, G = 150 μ m.

<https://doi.org/10.1371/journal.pone.0232807.g004>

From this analysis, we found that ~75% of DKO mice lacked AR protein expression at 25 weeks, but all of the HET and WT mice retained AR expression at this timepoint (Fig 5C). At 40 weeks, ~50% HET mice and less than 25% of WT mice showed loss of AR expression. Consistent with the observation that tumors from the castrate DKO mice exhibited androgen-insensitive growth also lacked AR expression (S3C Fig). However, we did not observe a significant difference in the expression of the AR target genes *MsmB* and *Apof* when comparing DKO and WT mice at 25 weeks (Fig 5D) [23, 24].

Discussion

Here we describe a Pb-Cre mediated *Pten;Trp53* double knockout mouse model of prostate cancer with a bioluminescent reporter for non-invasive monitoring of tumor growth. Our model showed accelerated tumor growth and mortality of the DKO mice as compared to HET and WT mice. While at approximately 25 weeks of age the HET mice were more like the WT

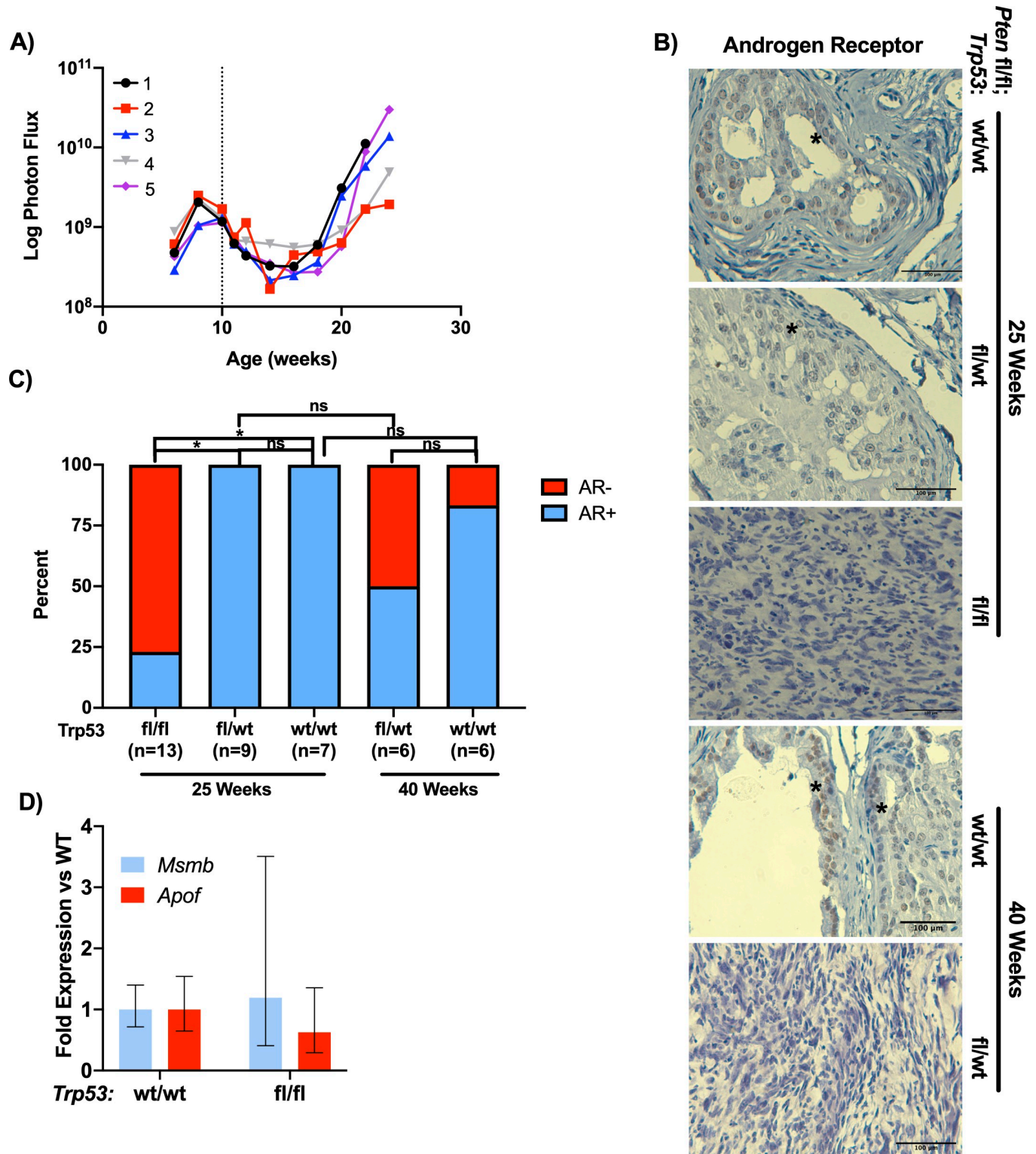


Fig 5. Loss of Trp53 and Pten results in castrate resistant disease. (A) BLI signal of a separate cohort of DKO mice that were castrated at 10 weeks of age (dotted line). Signal shows significant decrease immediately post-castration but over time recovers to levels of non-castrated counterparts. (B) Immunostaining of DKO, HET, and WT tissue at 25 weeks of age for AR. Bar = 100 μ m. (C). Analysis of (B) (*p < 0.05; Chi-Square with Bonferroni correction). (D) RT-qPCR data for AR target gene expression in WT and DKO mice at 25 weeks (p > 0.05, n = 5 per genotype).

<https://doi.org/10.1371/journal.pone.0232807.g005>

knockout mice, analysis of tissue collected at necropsy demonstrated that by 40 weeks of age the HET mice had progressed and became similar to the DKO mice. Necropsy tissue from both the DKO and HET mice showed that tumors had sarcomatoid pathology. This is a rare, undifferentiated and mesenchymal prostate pathology (<1% of prostate cancer tumors) that is considered to be highly aggressive [25–27]. The loss of p53 function may be associated with the development of sarcomatoid tumors in patients. Case studies have reported strong nuclear accumulation of p53 in the sarcomatoid regions of the tumor, consistent with oncogenic dominant-negative or gain-of-function mutations in p53 [28], whereas adenocarcinoma typically lacks strong p53 staining [29, 30]. In addition to the accumulation of p53, it has been demonstrated that the sarcomatoid portion of a prostate tumor lacks AR staining [31].

Sarcomatoid prostate cancer has been previously observed in *Trp53;Pten* prostate KO mice. In a report from Martin et. al. the authors noted that the progression of prostate tumors from Pb-Cre mediated knockout of *Trp53;Pten* resulted in a complete penetrance of spindle cell carcinoma or sarcomatoid pathology for mice between 26–30 weeks [12]. They also noted that the regions containing spindle cell carcinoma had low or undetectable AR expression [12]. Our results are consistent with these findings, as pathological analysis of necropsy tissue from our DKO mice displayed sarcomatoid features with most tumors lacking AR staining. However, our analysis of AR target genes *MsmB* and *Apof* did not demonstrate a significant difference in expression between the WT and DKO mice [23, 24]. This could be due to not utilizing laser capture microdissection to isolate tissue for mRNA analysis and thus the AR signal is diluted in the WT group due to stromal contamination. Additionally, due to reciprocal feedback between PI3K and AR signaling it is possible that the AR transcriptional output in *Pten* knockout animals is reduced below the level necessary to detect meaningful differences in expression across different *Trp53* genotypes, in spite of the differences in AR protein expression observed [32, 33].

While we were unable to demonstrate a difference in AR target gene expression between WT and DKO mice at 25 weeks, we were able to demonstrate a correlation of AR protein loss with the sarcomatoid histopathology. Utilizing BLI, we were able to determine that the DKO mice were initially responsive to castration but developed castrate-resistant disease 5 weeks later, which has not been previously reported in primary tumors. The age for the onset of tumor growth in castrated DKO mice (18 weeks) is consistent with the age in which the Martin study observed sarcomatoid pathology [12]. This association of loss of AR staining and sarcomatoid pathology was also observed in the tissue from the HET mice at 40 weeks of age. These tumors were similar to the tumors from DKO mice, as all tumors presented as sarcomatoid and 50% did not stain for AR. Given the reduced AR protein expression in sarcomatoid tumors and that the castrate DKO mice all had sarcomatoid pathology, it is likely that the rapid onset of castrate-resistant tumor growth was due to the progression of the prostate cancer to a sarcomatoid pathology. While the development of sarcomatoid pathology under castrate levels of androgen is interesting, it is still unknown what events lead to the formation of this disease state.

Another interesting aspect of this model is the association between the sarcomatoid pathology and EMT. In both the Martin study and case reports from patients, the sarcomatoid regions stained strongly for vimentin expression [12, 29]. Vimentin, along with Zeb1, are widely regarded as markers of EMT and have been implicated in the development of metastatic disease in many cancers, including prostate [34]. Our results show increased expression of both proteins in DKO tumors, and indeed we have shown that the expression of these proteins occurs within cells on adjacent serial sections if not the same cell. Interestingly EMT-like characteristics may result from the reduction of AR signaling in the sarcomatoid tumors. It has been demonstrated that androgen deprivation leads to elevated expression of EMT

markers in both normal and cancerous prostate tissue [35]. Moreover, Zeb1 and AR may regulate each other through mutually antagonistic processes [35].

Despite the presence of EMT markers in the sarcomatoid tumors, neither in the earlier reports nor in our study were distant metastases detected [11, 12]. Even with the addition of a bioluminescent reporter, we were able to detect only bioluminescent-positive tumor deposits that represented local invasion into peri-lymphatic fat as well as peritoneal seeding with tumor found on the pancreas. However, we cannot rule out the possibility that we did not detect micrometastatic disease in some organs which lacked sufficient BLI signal for detection because we did not exhaustively section metastatic end organs without BLI signal. In spite of the inability of BLI to detect metastatic disease in the model reported here, we believe there is utility in non-invasive, bioluminescent monitoring in the detection of distant, and potentially very small volume, metastatic disease. Moreover, the results from our study underscores the importance of validating BLI signal with histopathology.

For distant metastases to occur in the context of *Trp53;Pten* prostate-specific deletion, additional genes may need to be disrupted, such as *Rb1* or *Smad4* [13, 36, 37]. However, expression of EMT markers Zeb1 and vimentin suggests metastatic potential in this model, and certainly correlates with more aggressive disease including castrate resistance. Additionally, the trend for an increase in the expression of NE markers also suggests that this model would result in metastatic disease. There are at least two additional aspects of this model which may contribute to the lack of observed metastatic disease. First, because *Trp53;Pten* are deleted in the entire prostatic epithelium, the subsequent tumors in this model are rapidly fatal, likely from large tumor masses and urinary obstruction, which limits the time for progression of disease. To circumvent these problems, somatic deletion of Pten and Trp53 may provide a new direction. Indeed, a virally-introduced, Cre-mediated deletion of *Pten* and *Trp53* in mouse prostates has reportedly produced reliable metastasis [37]. Second, the host strain of the model may influence metastatic potential [6]. It has been shown that normal prostate tissue from different strains have alterations in expression of genes such as MMP7 and prostate specific stem cell antigen [38]. Moreover, BALB/c mice have loss of p16^{Ink4a}, which could alter metastatic potential by dysregulation of the Rb pathway [39]. Evaluating the loss of *Trp53;Pten* function across a range of host strains may elucidate this possibility and lead to the identification of metastasis modifier genes.

Supporting information

S1 Fig. Double knockout mice have accelerated tumor growth. (A) Graph of the exponential growth rate for each mouse from the Pten fl/fl; Trp53: wt/wt, fl/wt, and fl/fl groups. Blue line is the mean with grey boxes outlining the 95% confidence intervals. (B) Gross anatomical image of prostate tumor from a DKO mouse at endpoint (approximately 25 weeks). A blood-filled seminal vesicle is evident at the top right of the image. (C) Gross anatomical image of prostate from WT (Pten only knockout) mouse at approximately 25 weeks. Note in this specimen seminal vesicles are readily apparent.

(TIF)

S2 Fig. Analysis of EMT in WT and HET mice at 40 weeks of age. (A) Images of sections stained for Zeb1 and vimentin in WT and HET mice at 40 weeks, asterisk designates regions of positivity. Bar = 100 μ m (B) Analysis of EMT status in these mice at this time point ($p > 0.05$, Chi-Square test).

(TIF)

S3 Fig. Histopathology of castrate DKO mice. (A, B) H&E stain showing sarcomatoid carcinoma, similar to the non-castrated DKO mice. Yellow box in (A) is enlarged in (B) to show sarcomatoid architecture. (C) Immunostaining for AR. Bar = 150 μ m. (TIF)

Acknowledgments

We would like to thank Sophia Peterson for assistance with histopathology and Dr. Jennifer Richer, University of Colorado at Denver, for generously providing the Zeb1 antibody.

Author Contributions

Conceptualization: Nadine Bannick, Robert Svensson, Michael D. Henry.

Data curation: Courtney Yong, Devon L. Moose, Nadine Bannick, Wade R. Gutierrez, Marion Vanneste, James A. Brown, Rebecca D. Dodd, Michael D. Henry.

Formal analysis: Courtney Yong, Devon L. Moose, Patrick Breheny, Michael B. Cohen, Michael D. Henry.

Funding acquisition: James A. Brown, Michael D. Henry.

Investigation: Courtney Yong, Nadine Bannick, Marion Vanneste, Michael D. Henry.

Project administration: Michael D. Henry.

Resources: Rebecca D. Dodd.

Supervision: Michael D. Henry.

Visualization: Courtney Yong.

Writing – original draft: Courtney Yong, Devon L. Moose, Michael D. Henry.

Writing – review & editing: Courtney Yong, Devon L. Moose, Nadine Bannick, Wade R. Gutierrez, Marion Vanneste, Robert Svensson, Patrick Breheny, James A. Brown, Rebecca D. Dodd, Michael B. Cohen, Michael D. Henry.

References

1. Bashir MN (2015) Epidemiology of Prostate Cancer. *Asian Pac J Cancer Prev* 16: 5137–5141. <https://doi.org/10.7314/apjcp.2015.16.13.5137> PMID: 26225642
2. Siegel RL, Miller KD, Jemal A (2019) Cancer statistics, 2019. *CA Cancer J Clin* 69: 7–34. <https://doi.org/10.3322/caac.21551> PMID: 30620402
3. Cancer Genome Atlas Research N (2015) The Molecular Taxonomy of Primary Prostate Cancer. *Cell* 163: 1011–1025. <https://doi.org/10.1016/j.cell.2015.10.025> PMID: 26544944
4. Abida W, Cyrta J, Heller G, Prandi D, Armenia J, et al. (2019) Genomic correlates of clinical outcome in advanced prostate cancer. *Proceedings of the National Academy of Sciences* 116: 11428.
5. Greenberg NM, DeMayo F, Finegold MJ, Medina D, Tilley WD, et al. (1995) Prostate cancer in a transgenic mouse. *Proc Natl Acad Sci U S A* 92: 3439–3443. <https://doi.org/10.1073/pnas.92.8.3439> PMID: 7724580
6. Gingrich JR, Barrios RJ, Morton RA, Boyce BF, DeMayo FJ, et al. (1996) Metastatic prostate cancer in a transgenic mouse. *Cancer Res* 56: 4096–4102. PMID: 8797572
7. Kaplan-Lefko PJ, Chen T-M, Ittmann MM, Barrios RJ, Ayala GE, et al. (2003) Pathobiology of autochthonous prostate cancer in a pre-clinical transgenic mouse model. *The Prostate* 55: 219–237. <https://doi.org/10.1002/pros.10215> PMID: 12692788
8. Grabowska MM, DeGraff DJ, Yu X, Jin RJ, Chen Z, et al. (2014) Mouse models of prostate cancer: picking the best model for the question. *Cancer Metastasis Rev* 33: 377–397. <https://doi.org/10.1007/s10555-013-9487-8> PMID: 24452759

9. Wang S, Gao J, Lei Q, Rozengurt N, Pritchard C, et al. (2003) Prostate-specific deletion of the murine Pten tumor suppressor gene leads to metastatic prostate cancer. *Cancer Cell* 4: 209–221. [https://doi.org/10.1016/s1535-6108\(03\)00215-0](https://doi.org/10.1016/s1535-6108(03)00215-0) PMID: 14522255
10. Svensson RU, Haverkamp JM, Thedens DR, Cohen MB, Rattliff TL, et al. (2011) Slow disease progression in a C57BL/6 pten-deficient mouse model of prostate cancer. *Am J Pathol* 179: 502–512. <https://doi.org/10.1016/j.ajpath.2011.03.014> PMID: 21703427
11. Chen Z, Trotman LC, Shaffer D, Lin HK, Dotan ZA, et al. (2005) Crucial role of p53-dependent cellular senescence in suppression of Pten-deficient tumorigenesis. *Nature* 436: 725–730. <https://doi.org/10.1038/nature03918> PMID: 16079851
12. Martin P, Liu Y-N, Pierce R, Abou-Kheir W, Casey O, et al. (2011) Prostate Epithelial Pten/TP53 Loss Leads to Transformation of Multipotential Progenitors and Epithelial to Mesenchymal Transition. *The American Journal of Pathology* 179: 422–435. <https://doi.org/10.1016/j.ajpath.2011.03.035> PMID: 21703421
13. Ku SY, Rosario S, Wang Y, Mu P, Seshadri M, et al. (2017) Rb1 and Trp53 cooperate to suppress prostate cancer lineage plasticity, metastasis, and antiandrogen resistance. *Science* 355: 78–83. <https://doi.org/10.1126/science.aah4199> PMID: 28059767
14. Safran M, Kim WY, Kung AL, Horner JW, DePinho RA, et al. (2003) Mouse reporter strain for noninvasive bioluminescent imaging of cells that have undergone Cre-mediated recombination. *Mol Imaging* 2: 297–302. <https://doi.org/10.1162/153535003322750637> PMID: 14717328
15. Wu X, Wu J, Huang J, Powell WC, Zhang J, et al. (2001) Generation of a prostate epithelial cell-specific Cre transgenic mouse model for tissue-specific gene ablation. *Mech Dev* 101: 61–69. [https://doi.org/10.1016/s0925-4773\(00\)00551-7](https://doi.org/10.1016/s0925-4773(00)00551-7) PMID: 11231059
16. Lesche R, Groszer M, Gao J, Wang Y, Messing A, et al. (2002) Cre/loxP-mediated inactivation of the murine Pten tumor suppressor gene. *Genesis* 32: 148–149. <https://doi.org/10.1002/gene.10036> PMID: 11857804
17. Buchakjian MR, Merritt NM, Moose DL, Dupuy AJ, Tanas MR, et al. (2017) A Trp53fl/flPtenfl/fl mouse model of undifferentiated pleomorphic sarcoma mediated by adeno-Cre injection and in vivo bioluminescence imaging. *PLoS One* 12: e0183469. <https://doi.org/10.1371/journal.pone.0183469> PMID: 28841687
18. Ullman-Cullere MH, Foltz CJ (1999) Body Condition Scoring: A Rapid and Accurate Method for Assessing Health Status in Mice. *Laboratory Animal Science* 49: 319–323. PMID: 10403450
19. Spoelstra NS, Manning NG, Higashi Y, Darling D, Singh M, et al. (2006) The transcription factor ZEB1 is aberrantly expressed in aggressive uterine cancers. *Cancer Res* 66: 3893–3902. <https://doi.org/10.1158/0008-5472.CAN-05-2881> PMID: 16585218
20. Miller MR, Ma D, Schappet J, Breheny P, Mott SL, et al. (2015) Downregulation of dystroglycan glycosyltransferases LARGE2 and ISPD associate with increased mortality in clear cell renal cell carcinoma. *Molecular cancer* 14: 141–141. <https://doi.org/10.1186/s12943-015-0416-z> PMID: 26220087
21. Park JW, Lee JK, Witte ON, Huang J (2017) FOXA2 is a sensitive and specific marker for small cell neuroendocrine carcinoma of the prostate. *Modern pathology: an official journal of the United States and Canadian Academy of Pathology, Inc* 30: 1262–1272.
22. Epstein JI, Amin MB, Beltran H, Lotan TL, Mosquera J-M, et al. (2014) Proposed morphologic classification of prostate cancer with neuroendocrine differentiation. *The American journal of surgical pathology* 38: 756–767. <https://doi.org/10.1097/PAS.0000000000000208> PMID: 24705311
23. Heemers HV, Regan KM, Schmidt LJ, Anderson SK, Ballman KV, et al. (2009) Androgen modulation of coregulator expression in prostate cancer cells. *Molecular endocrinology (Baltimore, Md)* 23: 572–583.
24. Zhang M, Suarez E, Vasquez JL, Nathanson L, Peterson LE, et al. (2019) Inositol polyphosphate 4-phosphatase type II regulation of androgen receptor activity. *Oncogene* 38: 1121–1135. <https://doi.org/10.1038/s41388-018-0498-3> PMID: 30228349
25. Markowski MC, Eisenberger MA, Zahurak M, Epstein JI, Paller CJ (2015) Sarcomatoid Carcinoma of the Prostate: Retrospective Review of a Case Series From the Johns Hopkins Hospital. *Urology* 86: 539–543. <https://doi.org/10.1016/j.urology.2015.06.011> PMID: 26126695
26. Inamura K (2018) Prostatic cancers: understanding their molecular pathology and the 2016 WHO classification. *Oncotarget* 9: 14723–14737. <https://doi.org/10.18632/oncotarget.24515> PMID: 29581876
27. Hansel DE, Epstein JI (2006) Sarcomatoid carcinoma of the prostate: a study of 42 cases. *Am J Surg Pathol* 30: 1316–1321. <https://doi.org/10.1097/O1.pas.0000209838.92842.bf> PMID: 17001164
28. Kluth M, Harasimowicz S, Burkhardt L, Grupp K, Krohn A, et al. (2014) Clinical significance of different types of p53 gene alteration in surgically treated prostate cancer. *Int J Cancer* 135: 1369–1380. <https://doi.org/10.1002/ijc.28784> PMID: 24523142

29. Acosta AM, Senseng C, Kim G, Sekosan M, Ree N (2016) Sarcomatoid carcinoma of the prostate with adenocarcinoma, squamous cell carcinoma, and heterologous components. *APMIS* 124: 719–722. <https://doi.org/10.1111/apm.12548> PMID: 27197712
30. Delahunt B, Eble JN, Nacey JN, Grebe SK (1999) Sarcomatoid carcinoma of the prostate: progression from adenocarcinoma is associated with p53 over-expression. *Anticancer Res* 19: 4279–4283. PMID: 10628387
31. Salvi S, Casadio V, Martignano F, Gurioli G, Tumedei MM, et al. (2018) Carcinosarcoma of the prostate: case report with molecular and histological characterization. *Int J Biol Markers* 33: 540–544. <https://doi.org/10.1177/1724600818791463> PMID: 30101629
32. Carver BS, Chapinski C, Wongvipat J, Hieronymus H, Chen Y, et al. (2011) Reciprocal feedback regulation of PI3K and androgen receptor signaling in PTEN-deficient prostate cancer. *Cancer cell* 19: 575–586. <https://doi.org/10.1016/j.ccr.2011.04.008> PMID: 21575859
33. Mulholland DJ, Tran LM, Li Y, Cai H, Morim A, et al. (2011) Cell autonomous role of PTEN in regulating castration-resistant prostate cancer growth. *Cancer cell* 19: 792–804. <https://doi.org/10.1016/j.ccr.2011.05.006> PMID: 21620777
34. Nauseef JT, Henry MD (2011) Epithelial-to-mesenchymal transition in prostate cancer: paradigm or puzzle? *Nat Rev Urol* 8: 428–439. <https://doi.org/10.1038/nrurol.2011.85> PMID: 21691304
35. Sun Y, Wang BE, Leong KG, Yue P, Li L, et al. (2012) Androgen deprivation causes epithelial-mesenchymal transition in the prostate: implications for androgen-deprivation therapy. *Cancer Res* 72: 527–536. <https://doi.org/10.1158/0008-5472.CAN-11-3004> PMID: 22108827
36. Ding Z, Wu CJ, Chu GC, Xiao Y, Ho D, et al. (2011) SMAD4-dependent barrier constrains prostate cancer growth and metastatic progression. *Nature* 470: 269–273. <https://doi.org/10.1038/nature09677> PMID: 21289624
37. Cho H, Herzka T, Zheng W, Qi J, Wilkinson JE, et al. (2014) RapidCaP, a novel GEM model for metastatic prostate cancer analysis and therapy, reveals myc as a driver of Pten-mutant metastasis. *Cancer Discov* 4: 318–333. <https://doi.org/10.1158/2159-8290.CD-13-0346> PMID: 24444712
38. Bianchi-Frias D, Pritchard C, Mecham BH, Coleman IM, Nelson PS (2007) Genetic background influences murine prostate gene expression: implications for cancer phenotypes. *Genome Biol* 8: R117. <https://doi.org/10.1186/gb-2007-8-6-r117> PMID: 17577413
39. Zhang S, Ramsay ES, Mock BA (1998) Cdkn2a, the cyclin-dependent kinase inhibitor encoding p16INK4a and p19ARF, is a candidate for the plasmacytoma susceptibility locus, Pctr1. *Proceedings of the National Academy of Sciences of the United States of America* 95: 2429–2434. <https://doi.org/10.1073/pnas.95.5.2429> PMID: 9482902